Original Research

Brake wear-derived particles: Single-particle mass spectral signatures and real-world emissions

Jiayuan Liu, Jianfei Peng[*], Zhengyu Men, Tiange Fang, Jinsheng Zhang, Zhuofei Du, Qijun Zhang, Ting Wang, Lin Wu, Hongjun Mao

Tianjin Key Laboratory of Urban Transport Emission Research, College of Environmental Science and Engineering, Nankai University, Tianjin, 300071, China

ARTICLE INFO

ABSTRACT

Brake wear is an important but unregulated vehicle-related source of atmospheric particulate matter (PM). The single-particle spectral fingerprints of brake wear particles (BWPs) provide essential information for understanding their formation mechanism and atmospheric contributions. Herein, we obtained the single-particle mass spectra of BWPs by combining a brake dynamometer with an online single particle aerosol mass spectrometer and quantified real-world BWP emissions through a tunnel observation in Tianjin, China. The pure BWPs mainly include three distinct types of particles, namely, Ba-containing particles, mineral particles, and carbon-containing particles, accounting for 44.2%, 43.4%, and 10.3% of the total BWP number concentration, respectively. The diversified mass spectra indicate complex BWP formation pathways, such as mechanical, phase transition, and chemical processes. Notably, the mass spectra of Ba-containing particles are unique, which allows them to serve as an excellent indicator for estimating ambient BWP concentrations. By evaluating this indicator, we find that approximately 4.0% of the PM in the tunnel could be attributable to brake wear; the real-world fleet-average emission factor of 0.28 mg km^{-1} veh^{-1} is consistent with the estimation obtained using the receptor model. The results presented herein can be used to inform assessments of the environmental and health impacts of BWPs to formulate effective emissions control policies.

© 2023 The Authors. Published by Elsevier B.V. on behalf of Chinese Society for Environmental Sciences, Harbin Institute of Technology, Chinese Research Academy of Environmental Sciences. This is an open access article under the CC BY-NC-ND license (http://creativecommons.org/licenses/by-nc-nd/4.0/).

1. Introduction

Road traffic emissions have been a major focus of environmental management efforts over the past several decades [1–3]. Legislation and technological innovation have been effective in terms of driving down the emissions of exhaust PM$_{2.5}$ (particulate matter with aerodynamic diameter $\leq$ 2.5 μm) [4–6]. However, non-exhaust PM$_{2.5}$ emissions, including brake wear, tire wear, and road wear [7,8], are currently unrestricted and account for increasing proportions of total road traffic emissions [9]. In addition, the implementation of electric vehicles may increase the contribution of non-exhaust particles owing to the higher weight of electric vehicles [10]. The United Kingdom's National Atmospheric Emissions Inventory (NAEI) estimated that vehicular non-exhaust PM emissions exceeded exhaust emissions in 2014 and have since

continued to increase [11]. Moreover, non-exhaust particles may have more considerable public health impacts than exhaust particles owing to their higher oxidative potential [12]. Therefore, regulating non-exhaust emissions is crucial [13].

Brake wear is a key source of non-exhaust emissions, especially in heavy traffic areas [14,15]. For example, Hasheminassab et al. [16] found that brake wear particles (BWPs) contributed between 7.3% and 19.1% of the total suspended particulate matter in Paramount, California. According to the Air Quality in Europe-2019 Report, 7% and 9% of the vehicle-related PM$_{10}$ and PM$_{2.5}$ emissions, respectively, could be attributed to BWPs [17]. Jeong et al. [18] reported that the contribution of brake wear to non-exhaust PM$_{2.5}$ emissions was higher at highway sites (64%) than at downtown sites (45%). Grigoratos and Martini suggested that in urban environments, BWPs accounted for up to 55% and 21% of the total non-exhaust and traffic-related PM$_{10}$ emissions, respectively [5].

BWPs are generated from the mechanical friction between the brake pad and the rotating disc or drum during the vehicle braking process [19,20]. Disc brakes, which comprise abradable brake pads

that run on brake discs, are currently the most common type of braking system [21]. The brake linings include five components: fillers, abrasives, reinforcing fibers, binders, and lubricants. The chemical composition of commercial brake lining varies significantly according to the brake pad specifications and manufacturers, thus leading to a wide range of BWP chemical compositions [5,22]. Studies have shown that BWPs is a significant source of redox-active and toxic metals (e.g., Ba, Cu, Sb, Zr, Zn) in the atmosphere, which can adversely affect public health [23,24].

Brake wear emissions are influenced by various factors, including driving styles, braking intensity, brake temperature, friction materials, and quality of the brake system [25,26]. The most common ways to estimate brake wear-derived PM emissions are via laboratory dynamometer experiments [27], on-board measurements [28], or receptor modeling [29,30]. Currently, reliable quantitative data related to brake wear emissions are limited. Brake dynamometers have been used in previous BWP emissions studies to determine the features of BWPs, but this approach cannot accurately represent real-world braking conditions [31]. In contrast, on-board measurements estimate emissions under real-world driving conditions but can only represent BWP emissions from limited vehicles, rather than a vehicle fleet [32]. Receptor models, such as Positive Matrix Factorization (PMF) and Chemical Mass Balance (CMB), have also been used to relate chemical component data to the source contributions [8]. However, receptor models are limited by the input parameters and have difficulty separating individual non-exhaust sources (e.g., differentiating brake wear from road dust) [33]. To date, few studies have accurately quantified the contribution of brake wear to ambient PM through real-world measurements [7,34].

Single-particle chemical composition analysis provides valuable information for identifying the sources of particles in the atmosphere. Single particle aerosol mass spectrometry (SPAMS) is widely used to study source and ambient particles because it enables instantaneous and simultaneous measurements of the aerodynamic diameter and chemical composition of individual particles [35,36]. For example, Xu et al. [37] studied single-particle mass spectral signatures and sizes of PM emitted when burning biomass or coal. Chen et al. [38] used a SPAMS to compare ambient loess particles with dust particles from different sources (e.g., urban background, road, soil, and construction) to investigate the atmospheric cycles of loess particles in urban areas. Yang et al. [39] used SPAMS to group vehicular-emitted particles in a tunnel into four categories: ECOC (elemental and organic carbon), NaK, Metal, and PAHs (polycyclic aromatic hydrocarbons). Furthermore, source apportionment methods based on SPAMS have been developed to identify the origins of individual particles [40]. For example, Fu et al. [41] used SPAMS in combination with an Art-2a neural network algorithm to apportion the marine aerosols over the East China Seas into secondary-containing, aged sea salt, soot-like, biomass burning, fresh sea salt, and lead-containing particles. Peng et al. [42] developed a new method (SPAMS-RM) that employed the receptor model Multilinear Engine-2 (ME2) on the dataset of SPAMS to identify particle sources. To date, SPAMS has been used to analyze particles emitted from coal burning, dust, industrial plants, and vehicle exhaust [43−45]. However, limited information is available regarding single-particle spectra of BWPs [46].

In this study, we investigated the single-particle mass spectra features of BWPs by combining a brake dynamometer and SPAMS and quantified real-world BWP emissions through a tunnel observation. We first characterized individual BWPs from laboratory experiments to determine a suitable indicator for BWPs. Subsequently, we conducted a two-week SPAMS study in Tianjin, China, to characterize atmospheric PM in a tunnel and identify BWPs in

the vehicle-dominated environment based on the mass spectral fingerprints obtained in the laboratory experiments. Finally, we established a method for quantifying the BWP concentration in the tunnel and estimating the emission factor of brake wear. To our knowledge, this study represents the first attempt to quantify the contribution of BWP emissions based on online single-particle measurements, and therefore the results presented herein provide a reference for accurate assessments and control of brake emissions.

2. Materials and methods

2.1. Laboratory experiments investigating brake wear emissions

Braking tests were performed using a brake dynamometer at the China Automotive Technology and Research Center. Because the exact market share proportions of brake pads are currently unavailable, we selected brake pads based on the corresponding market shares of vehicle brands in China. Five brake pad disc types were evaluated in the brake wear testing experiments. These five types of brake pads belonged to five distinct vehicle models in the top market-share brands in China [47]. Therefore, we assumed that the selected brake pads roughly represent the actual brake pads used in the majority of the vehicle fleet in China. More information about the five brake assemblies is presented in Table S1. During the braking tests, we altered the driving conditions by changing the initial speed and rate of deceleration. For each brake pad, 1400-s orthogonal tests were performed at initial speeds of 40, 60, and 120 km h^{-1} and braking deceleration rates of 1, 2, 3, 5, and 7 m s^{-2}. Each braking test was repeated ten times for each disc-pad assembly [27]. Particles generated during these braking tests were collected and evenly mixed for subsequent SPAMS analysis. Details related to the collection and treatment of BWPs are provided in the Supplementary Materials.

2.2. Tunnel measurements

Two-week-long tunnel observations were conducted in the Wujinglu Tunnel in Tianjin (117°12′15″ E, 39°8′31″ N) between August 27 and September 11, 2021 (Fig. 1). The tunnel is a three-lane, about 1 km long urban tunnel with an average daily traffic volume of 15 000 vehicles and an effective cross-sectional area of approximately 54 m^2. The vehicle speed in the tunnel is limited to 40 km h^{-1}. This tunnel is used by a high proportion of gasoline-fueled vehicles, many of which are small private cars. During the sampling period, the longitudinal jetting ventilation fan in the tunnel was turned off. Therefore, tunnel ventilation was mainly induced by the vehicles passing through the tunnel and the prevailing wind.

Three sampling sites (#1, #2, and #3 in Fig. 1) were set up in the Wujinglu Tunnel: the #1 site was approximately 45 m away from the tunnel entrance; the #3 site was approximately 50 m from the tunnel exit; and the #2 site was located between sites #1 and #3 at
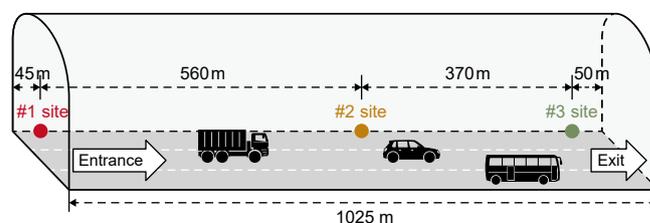
Fig. 1. Observation sites in the Wujinglu Tunnel.

respective distances of approximately 560 and 370 m. Measurement instruments were placed on the sidewalk on the left side of the tunnel at each sampling site. The SPAMS instrument (Hexin Analytical Instrument Co., Ltd., China) was placed at the #3 sampling site to measure the chemical composition and aerodynamic size of individual particles in the tunnel. During the observation period, the $PM_{2.5}$ (12-h samples) were continuously collected on polypropylene filters with a flow rate of 100 L min^{-1} using medium-volume air samplers (TH-150 A Tianhong, China) at the #1 and #2 sites. A total of 21 $PM_{2.5}$ samples were obtained. The elements related to brake wear (e.g., Ba, Cu, Fe, Zn) were analyzed by inductively-coupled plasma mass spectrometry (ICP-MS; Agilent 7900, USA). At the same time, real-time $PM_{2.5}$ mass concentrations were measured simultaneously by an air particulate matter monitor (Pegasor AQTM Urban, Finland) at sites #1 and #2. After the observations, the hourly number concentrations of particles in the tunnel (as measured by SPAMS) were scaled using a scanning mobility particle sizer (SMPS 3898 TSI, USA) and an aerodynamic particle sizer (APS 3321 TSI, USA). The detailed process is described in Section 2.4 (*vide infra*). Traffic data were measured using a roadside laser loop detector (AxleLight RLU11, Aozer, China) and a high-definition vehicle license plate recognition system (DS-TCG225-KN, Hikvision Inc.). The traffic flow, average speed, and vehicle types during the observation period are presented in Fig. S5. The meteorological parameters, including the temperature (T), relative humidity (RH), wind speed (WS), and wind direction (WD) were measured at sites #1 and #2 using two automatic weather stations (VAISALA WXT520, Finland). An ultrasonic gas flowmeter (Flowsic-200 SICK MAIHAK, Germany) was installed at the #2 site to measure the cross-sectional WS in the tunnel. The WD in the tunnel was generally constant and remained consistent with the direction of vehicle travel. The WS variations at the two sites were also relatively consistent, and the VAISALA and Flowsic 200 measurements showed good correlation (further information in the Supplementary Materials). Gaseous pollutants (e.g., NO_2, SO_2, and CO) were also measured simultaneously (Fig. S6).

2.3. Description of SPAMS

The operating principles of SPAMS have been reported previously [48,49]. Briefly, an aerodynamic lens is used as the particle interface, through which aerosols are drawn into the internal vacuum. Then, the focused particle beam passes through two continuous diode ND:YAG laser beams (532 nm) to determine the aerodynamic sizes of single particles. Subsequently, particles are ionized at the center of the ion source by a pulsed Nd:YAG laser (266 nm) to produce positive and negative ion fragments, which are analyzed via time-of-flight mass spectrometry. Thus, SPAMS can simultaneously detect the chemical compositions and particle diameters of single-particle aerosols in the range of 0.2−2.0 μm.

The collected SPAMS datasets were input into the Computational Continuation Core (COCO V1.4_p) toolkit based on MATLAB software for analysis and processing. An Adaptive Resonance Theory Neural Network Algorithm (ART-2a) was used to classify the pure BWPs. The parameters for the ART-2a analysis included a vigilance factor of 0.85, a learning rate of 0.05, and a maximum of 20 iterations. This algorithm could automatically group similar particles into the same category according to the type and intensity of their ion peaks in the particle mass spectrum.

2.4. Correction and quantification of SPAMS data

Despite its various advantages in terms of real-time single particle analysis and source identification, SPAMS has certain limitations related to the quantitative analysis of aerosols [50]: (1) its

ability to transport particles through the interface and detect the particles with two continuous sizing laser beams (transmission efficiency); (2) the different ratios of ionized particles (creating mass spectra) to sized particles during different periods (i.e., hit efficiency); and (3) the different detection sensitivities of the mass spectral ion signals for different chemical substances. Nevertheless, some studies have successfully obtained quantitative information from SPAMS by scaling and correcting the particle counts and ionic strengths by implementing reference instrument measurements (e.g., SMPS or APS) with hourly or higher time resolution [50,51]. The scaling approach used in this study considered two key parameters: the transmission efficiency and hit efficiency [50,52,53].

The transmission efficiency was determined by comparing the number concentrations of particles measured by SPAMS with those simultaneously measured by SMPS and APS. This strategy is effective because SMPS measures the electrical mobility diameter, which is different from the aerodynamic diameter measured by SPAMS and APS. To enable proper comparisons, the particle diameters obtained by SMPS were converted into aerodynamic diameters using equation (1) [54],

$$Da = Dm\sqrt{\frac{C_{Dm} \cdot \rho_{eff}}{C_{Da} \cdot \rho_0}} \tag{1}$$

where Da is the aerodynamic diameter; Dm is the electrical mobility diameter; C_{Dm} and C_{Da} are the Cunningham slip correction factors of the electrical mobility diameter and aerodynamic diameter, respectively; ρ_0 is the standard density (1 g cm^{-3}); and ρ_{eff} is the effective density. Effective density typically reflects the average density and shape of the particles [55]. In this study, a density of $\rho_{eff} = 1.7$ g cm^{-3} was used, which is consistent with the results of previous aerosol density studies in Chinese cities, including Beijing and Shanghai [56,57]. After converting the SMPS-derived diameters, the SMPS and APS size distribution data were merged with the overlapping part of the size distribution obtained from SMPS data (Fig. S2).

The hourly particle number concentrations from SPAMS analysis were divided into 18 bins from 0.2 to 2.0 μm (Da), and the transmission efficiency ($1/E$) of each bin was calculated. Specifically, the number concentrations of the first seven SPAMS bins (from 0.2 to 0.9 μm) were compared with SMPS data, and the last 11 bins (from 0.9 to 2.0 μm) were compared with APS data. To complete this analysis, the SMPS and APS particle size bins were merged, and the time resolution of the data was converted to 1 h. The inverse particle transmission efficiency (E) of SPAMS was calculated using equation (2):

$$E_b = \frac{N_{b,\text{SMPS\&APS}}}{N_{b,\text{SIZE}}} \tag{2}$$

where $N_{b,\text{SMPS\&APS}}$ is the number concentration of SMPS or APS, and $N_{b,\text{SIZE}}$ is the SPAMS number concentration in a given size bin b.

Considering the particle loss during the "diameter-ionization" process, the hit efficiency (H) during each hour was calculated using equation (3) to indirectly correct the chemical deviation of the SPAMS data,

$$H_b = \frac{N_{b,\text{mass}}}{N_{b,\text{SIZE}}} \tag{3}$$

where $N_{b,\text{mass}}$ and $N_{b,\text{SIZE}}$ are the numbers of particles with mass spectra and particle size information obtained in a given size bin b. Studies have demonstrated that the chemical composition and particle size of aerosols have a significant influence on H [51];

moreover, H is also affected by meteorological factors, such as temperature and humidity [50].

As suggested by Zhou et al. [50], we used the obtained E and H parameters to scale the SPAMS data and convert the particle volume measured by SPAMS into the "ambient" particle volume. Particle volume can be calculated using equation (4),

$$V_{ks} = \sum_{b=1}^{18} \frac{\sum_i V_{i,k,b}}{H_b} E_b \tag{4}$$

where V_{ks} is the volume concentration of ambient particles containing component k; H_b and E_b are the average hit efficiency and inverse transmission efficiency in bin b, respectively; and $V_{i,k,b}$ represents the volume of an individual particle i containing species k in bin b, which can be calculated using equation (5):

$$V_i = \frac{\pi}{6} Dm^3 \tag{5}$$

To obtain mass concentration datasets of particles with a time resolution of 1 h, the volume concentration was converted into mass concentration using equation (6),

$$C_{ks} = \rho \cdot V_{ks} \tag{6}$$

where C_{ks} is the mass concentration of ambient particles containing component k, and ρ is the density of particles. In these calculations, we used density values of 1.7 g cm^{-3} for ambient PM, 2.5 g cm^{-3} for Ba-containing particles and mineral particles, and 1.4 g cm^{-3} for carbon-containing particles [58−60].

Owing to instrumental limitations, the scaled SPAMS data only cover the size range of 0.2−2.0 μm, which introduces uncertainty when comparing PM$_{2.5}$ filter data. Herein, we assumed that the proportion of Ba-containing particles by number in the range of 2.0−2.5 μm was equal to that in the range of 1.5−2.0 μm. On the basis of this assumption and considering the particle concentrations measured by APS in the range of 2.0−2.5 μm, we computed the number and volume concentrations of PM and Ba-containing particles in this size range. Therefore, the scaled particles were approximately extended from PM$_{2.0}$ to PM$_{2.5}$.

2.5. Mass concentration and emission factor calculations

The results of laboratory experiments identified Ba-containing particles as a good indication of BWPs that can be used to estimate brake wear emissions. The concentration of BWPs in the tunnel was calculated by multiplying the scaling factor by the mass concentration of Ba-containing particles according to equations (7) and (8),

$$C_{\text{Brake}} = C_{\text{Ba−containing}} \times F_{\text{scaling}} \tag{7}$$

$$F_{\text{scaling}} = 1 \Big/ R \tag{8}$$

where C_{Brake} and $C_{\text{Ba-containing}}$ are the mass concentrations of BWPs and Ba-containing particles in the tunnel, respectively ($C_{\text{Ba-containing}}$ was converted from the Ba-containing particle concentration measured by SPAMS using the quantitative method described in Section 2.4); and F_{scaling} is the scaling factor, which was determined based on the mass proportion of Ba-containing particles in pure BWPs measured in the laboratory (R).

The BWP concentration increments at the #3 site compared with the #2 site were used to calculate the real-world average fleet emission factor because they reflected the concentrations of particles originating from the internal sources of the tunnel.

Specifically, the emission factor of brake wear was calculated using the following distance-based equation [61,62],

$$EF_{\text{fleet}} = \frac{(C_{\text{Brake\_#3}} - C_{\text{Brake\_#2}}) \times A \times v \times t}{N \times L} \tag{9}$$

where EF_{fleet} is the emission factor of brake wear (mg km^{-1} veh^{-1}); $C_{\text{Brake\_#3}}$ is the BWP concentration at site #3 (mg m^{-3}), as calculated using equation (7); $C_{\text{Brake\_#2}}$ is the BWP concentration at site #2 (mg m^{-3}), as calculated using equations (10) and (11), below; A is the cross-sectional area of the tunnel (54 m^2); v is the wind speed parallel to the tunnel (m s^{-1}); t is the sampling duration (s); N is the total number of vehicles passing through the tunnel during the sampling period; and L is the distance between sites #2 and #3 (370 m).

This study assumed that the PM emitted by vehicles in the tunnel was uniform and the proportion of Ba in BWPs was relatively stable. Considering these assumptions and the filter sampling data at sites #1 and #2 sites, we can compute $C_{\text{Brake\_#2}}$ using equations (10) and (11),

$$\frac{C_{\text{Ba\_#2}} - C_{\text{Ba\_#1}}}{l_1} = \frac{C_{\text{Ba\_#3}} - C_{\text{Ba\_#2}}}{l_2} \tag{10}$$

$$\frac{C_{\text{Ba\_#2}}}{C_{\text{Brake\_#2}}} = \frac{C_{\text{Ba\_#3}}}{C_{\text{Brake\_#3}}} \tag{11}$$

where $C_{\text{Ba\_#1}}$ and $C_{\text{Ba\_#2}}$ represent the mass concentrations of Ba in PM$_{2.5}$ at sampling sites #1 and #2, respectively; $C_{\text{Ba\_#3}}$ is the Ba mass concentration at site #3, which was calculated using equation (10); l_1 is the distance between sites #1 and #2 (560 m); and l_2 is the distance between sites #2 and #3 (370 m).

3. Results and discussion

3.1. Single-particle chemical profiles of BWPs

A total of 24 090 pure BWPs were observed by SPAMS, approximately 7.2% of which were detected by the mass spectrometer for both positive and negative spectral measurements. Fig. 2 shows the size distribution and averaged mass spectra of the pure BWPs. For BWPs with size information (Fig. 2a), the peak appeared at 0.5−0.6 μm. Notably, the particle size distribution measured by SPAMS could differ slightly from the real situation because of the size-dependent detection efficiency of the method [44]. In the averaged mass spectra (Fig. 2b), ^{23}Na$^+$, ^{24}Mg$^+$, ^{27}Al$^+$, ^{39}K$^+$, ^{40}Ca$^+$, and ^{56}Fe$^+$ were the major signals in the positive SPAMS mass spectrum, and ^{16}O$^-$, ^{19}F$^-$, ^{24}C$_2^-$, ^{26}CN$^-$, ^{63}PO$_2^-$, and ^{79}PO$_3^-$ were the dominant signals in the negative spectrum. The mass spectral features of BWPs differ significantly from those of vehicle exhaust particles, which contain abundant carbon signals attributed to organic fragments and elemental carbon clusters [43]. In particular, the presence of certain Ba-ion signals (^{138}Ba$^+$, ^{154}BaO$^+$, ^{157}BaF$^+$) in the positive spectrum differentiates the spectrum from that of other known sources. Beddows et al. [46] used aerosol time-of-flight mass spectrometry (ATOFMS) with two inlet configurations (i.e., aerodynamic lens inlet and countersunk nozzle inlet) to sample BWPs. Consistent with our results, they observed peaks corresponding to ^{27}Al$^+$, ^{39}K$^+$, ^{56}Fe$^+$, ^{138}Ba$^+$, ^{154}BaO$^+$, ^{63}PO$_2^-$, and ^{79}PO$_3^-$ in the averaged mass spectrum.

To better understand the chemical characteristics and formation mechanism of BWPs, Art-2a was used to classify the pure BWPs detected with mass spectral information. Three types of BWPs (i.e., Ba-containing particles, mineral particles, and carbon-containing particles) were identified, as illustrated in Fig. 3. The mass
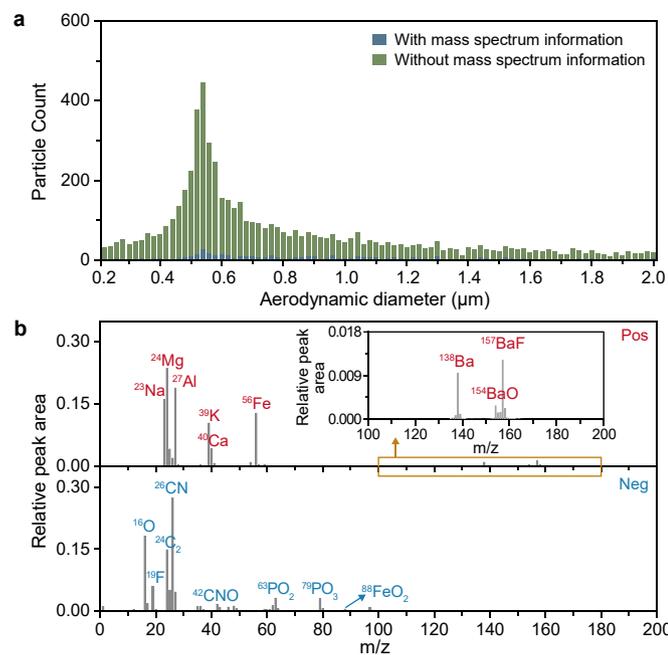
Fig. 2. Size and chemical profiles of pure BWPs. **a**, Size distribution of BWPs with (blue) and without (green) mass spectral information. **b**, Positive (top) and negative (bottom) mass spectra of BWPs.

spectrum of Ba-containing particles is characterized by strong positive peaks corresponding to metal components, including $^{23}Na^+$, $^{24}Mg^+$, $^{27}Al^+$, $^{39}K^+$, $^{40}Ca^+$, $^{56}Fe^+$, and Ba signals ($^{138}Ba^+$, $^{154}BaO^+$, and $^{157}BaF^+$), and negative signals corresponding to $^{26}CN^-$, $^{63}PO_2^-$, and $^{79}PO_3^-$ (Fig. 3a). The spectrum of mineral particles contains strong peaks associated with $^{23}Na^+$, $^{24}Mg^+$, $^{27}Al^+$, $^{16}O^-$, $^{19}F^-$, $^{24}C_2^-$, and $^{26}CN^-$ ions and weak peaks corresponding to $^{40}Ca^+$ and $^{56}Fe^+$ ions (Fig. 3b). The mass spectrum of carbon-containing particles is distinguished by the dominant presence of organic fragment peaks in both the positive and negative ion spectra, including higher-intensity signals for $^{24}C_2^+$, $^{25}C_2H^{+/-}$, $^{27}C_2H_3^{+/-}$, and $^{39}C_3H_3^+$.

The three particle types described above account for 97.9% of the BWPs in number, such that Ba-containing particles, mineral particles, and carbon-containing particles account for 44.2%, 43.4%, and 10.3%, respectively (Fig. 4a). Ba-containing particles and mineral particles account for a relatively large proportion of the particles in the size range of 1–2 μm (Fig. 4b). Additionally, the proportion of mineral particles (which may be generated from abrasives in the brake pads) increases with increasing particle size. In contrast, the fraction of carbon-containing particles is higher among particles with diameters less than 1 μm, and their proportion among particles with diameters of 0.2–0.5 μm is three times higher than that among particles with diameters of 1.5–2.0 μm. These differences in the particle size distribution indicate the diversified formation mechanisms of BWPs.

The chemical composition of BWPs largely depends on the material and specifications of brake pads, which are typically composed of steel fibers, graphite, wear-resistant agents, and resins [63]. For example, steel fibers (i.e., Fe) are the most abundant friction materials used in brake pads because they provide mechanical strength to the friction lining. Graphite is usually used as a lubricant, which affects the wear characteristics of the lining. Aluminum oxide (Al_2O_3) and iron oxide (Fe_2O_3) are the most common abrasive components. Barium sulfate ($BaSO_4$), magnesium oxide (MgO), and calcium carbonate ($CaCO_3$) are commonly used inorganic filler
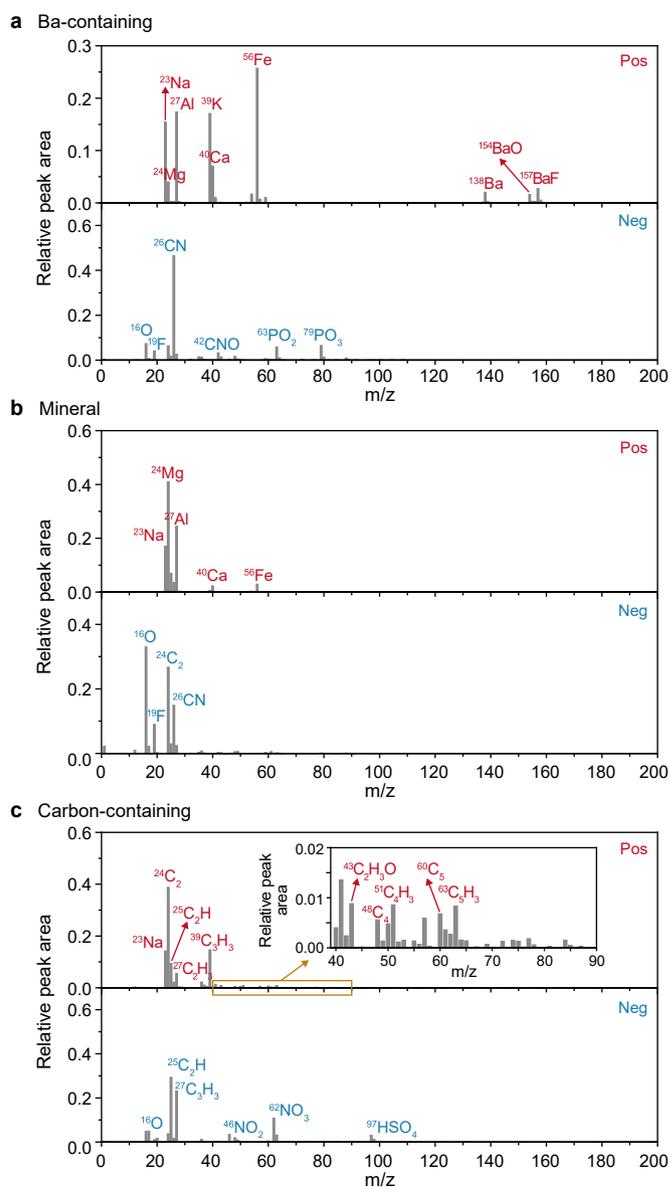
Fig. 3. Average positive and negative mass spectra of different types of BWPs. **a**, Ba-containing particles. **b**, Mineral particles. **c**, Carbon-containing particles.

materials that improve thermal and noise pad properties [5]. These chemical substances coexist in most brake pads and, as a result, they represent the major components of BWPs (see Fig. 2).

The materials in the brake pads are not homogeneously distributed, but rather, they exist as a mixture of many different ingredients. During a braking event, various BWP generation mechanisms, such as mechanical wear, coagulation, and/or chemical processes, produce particles with distinct chemical compositions [8]. For example, coarse particles are mainly produced by mechanical processes [64]. Mineral particles account for a significant proportion of large particles, which may mainly be derived from mechanical wear caused by braking. In addition to the mechanical wear process, the friction heat between the pads and rotating discs can release organic vapors. For example, our group's previous work indicated that volatilization and condensation of organic components in brake pads can significantly increase the production of nanoparticles during braking [27]. The present study also observed a high proportion of carbon-containing particles with
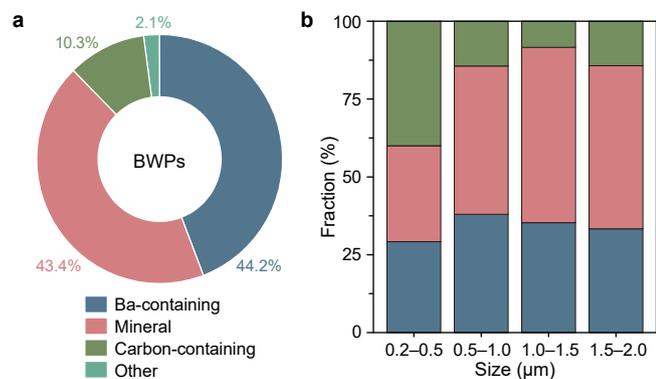
Fig. 4. The proportions (**a**) and size distributions (**b**) of major particle types in BWPs.

diameters $\leq$ 0.5 μm, indicating that these particles may form following the coagulation of nanoparticles generated from organic vapors.

Studies have shown that Ba rarely exists in PM derived from other sources, and therefore the presence of Ba-containing particles can be used as a reliable indicator of brake wear [5,65]. In the present study, Ba was selected as a quantitative indicator to identify BWPs in the tunnel monitored by SPAMS. We used the densities of 2.5, 2.5, and 1.4 g cm^{-3} to convert the SPAMS-determined numbers of Ba-containing, mineral, and carbon-containing particles in pure BWPs into mass values. The converted masses of these particle types accounted for 35.1%, 54.9%, and 9.1% of the total mass concentration, respectively. The $F_{scaling}$ was obtained from the mass proportion of Ba-containing particles in pure BWPs measured in the laboratory. The pure BWPs included 35.1% Ba-containing particles, corresponding to an $F_{scaling}$ of 2.8 (equation (8)), which was multiplied by the concentration of Ba-containing particles in the tunnel (measured by SPAMS) to determine brake wear-derived concentrations in the following calculation.

3.2. Features of ambient particles in the tunnel

During the tunnel observation period, a total of 6.9 million particles were detected by SPAMS, of which 691 658 particles contained positive and negative ion spectral information (average hit efficiency = 10.0%). The averaged mass spectra of the particles inside the tunnel are shown in Fig. 5. In the positive spectrum, the strongest signal corresponds to $^{39}K^+$, which is likely because of the high sensitivity of SPAMS to alkali metals [37]. The other dominant ions in the positive spectrum are EC (elemental carbon)-related
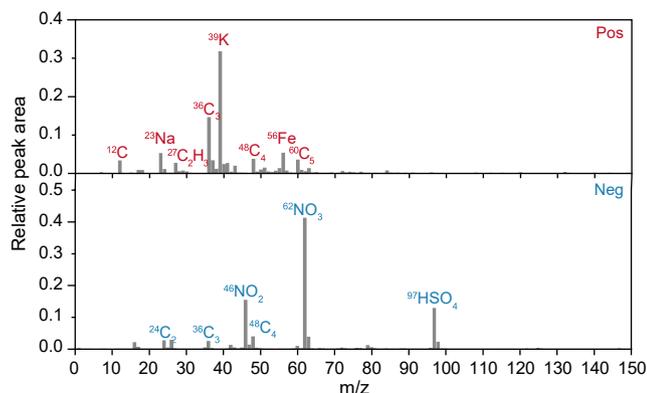
fragments (e.g., $^{12}C^+$, $^{36}C_3^+$, $^{48}C_4^+$, and $^{60}C_5^+$), which likely originated from vehicle exhaust emissions. Meanwhile, an $^{56}Fe^+$ signal appeared in the spectrum, indicating significant contributions from brake wear and road dust particles. The negative spectrum mainly includes EC-related fragments ($^{24}C_2^-$, $^{36}C_3^-$, and $^{48}C_4^-$) and secondary inorganic ions ($^{46}NO_2^-$, $^{62}NO_3^-$, and $^{97}HSO_4^-$), suggesting a significant influence of ambient aerosols on particles inside the tunnel.

According to the laboratory analysis, Ba-containing particles in the tunnel were identified by the marker ion at $m/z = 138$ (Ba$^+$), with a relative peak area larger than 0.5% of the total signals in the mass spectrum. Through this method, almost 4000 Ba-containing particles were detected during the tunnel observation, accounting for 0.5% of the total particles with mass spectral information. The averaged mass spectra and size distributions of Ba-containing particles are presented in Fig. 6. The specific signals corresponding to Ba ($^{138}Ba^+$, $^{154}BaO^+$) were clearly observed (Fig. 6a). The positive ion spectrum is dominated by strong $^{23}Na^+$, $^{24}Mg^+$, $^{27}Al^+$, $^{39}K^+$, $^{40}Ca^+$, $^{56}Fe^+$, $^{138}Ba^+$, $^{154}BaO^+$ and carbonaceous ($^{12}C^+$, $^{36}C_3^+$) peaks. Dominant peaks in the negative ion spectrum include secondary inorganic species ($^{46}NO_2^-$, $^{62}NO_3^-$, and $^{97}HSO_4^-$), followed by $^{16}O^-$, $^{24}C_2^-$, $^{26}CN^-$, $^{36}C_3^-$, $^{42}CNO^-$, $^{63}PO_2^-$, $^{79}PO_3^-$, and $^{88}FeO_2^-$. The Ba-containing particles were mainly smaller than 1 μm in diameter (peak between 0.5 and 0.6 μm) (Fig. 6b), which is consistent with the results of the laboratory experiment (Fig. 2a). Additionally, the proportion of Ba-containing particles increases in the larger size ranges, indicating that brake wear emissions likely contribute more to the formation of larger particles. Considering that Ba-containing particles observed inside the tunnel and in the laboratory exhibit similar mass spectral features and size distributions, it should be feasible to use Ba-containing particles measured by SPAMS as a quantitative indicator of BWPs in ambient air.

3.3. Quantification of BWP emissions under real-world conditions

The quantification of brake wear emissions in this work mainly involved three steps. First, the concentrations of Ba-containing particles and total particles (herein considered as PM$_{2.5}$) measured by SPAMS in the tunnel were scaled and converted into
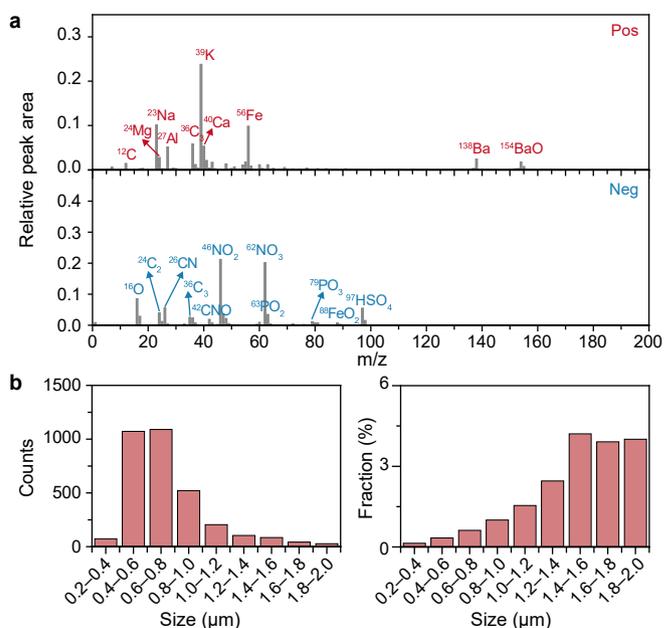
Fig. 6. Averaged mass spectra (**a**) and size distributions (**b**) of Ba-containing particles in the tunnel.

Fig. 5. Average mass spectra of ambient particles in the tunnel.

mass concentrations. Then, the BWP concentration and contribution to PM$_{2.5}$ in the tunnel environment were estimated based on the mass proportion of Ba-containing particles in pure BWPs determined in the laboratory experiment. Finally, a real-world fleet-averaged emission factor was determined by combining SPAMS data with filter data.

The mass concentration conversion method described in Section 2.4 was used to transform SPAMS data during the tunnel observation experiment. The average inverse particle transmission efficiencies (E) and hit efficiencies (H) of each size bin obtained in this study are presented in Fig. 7. We removed the hourly data with less than five particles in each particle size bin and were left with a total of 120 h of data to compute "E" (Fig. 7a) and 355 h of data to compute "H" (Fig. 7b). After scaling by "E" and "H", the particle volume ("size") measured by SPAMS was converted to the real ambient particle volume (equation (4)). Then, appropriate particle densities (2.5 g cm^{-3} for Ba-containing particles and 1.7 g cm^{-3} for ambient PM) were selected according to previous studies [58,59,66], and the volume concentration was converted into mass concentration (equation (6)). The mass concentrations of total particles (PM$_{2.5}$) and Ba-containing particles obtained following the conversion were 47.34 and 0.68 μg m^{-3}, respectively. Finally, by multiplying the $F_{scaling}$ (2.8; see Section 3.1) by the mass concentration of Ba-containing particles, the average BWP concentration in the tunnel during the sampling period was calculated to be 1.9 μg m^{-3}, accounting for 4.0% of PM$_{2.5}$. This proportion was consistent with that calculated using the receptor model, which

indicated that brake wear contributed to 1−5% of PM$_{2.5}$ [30].

The BWP concentration at site #3 was measured and quantified based on SPAMS data (average concentration = 1.9 μg m^{-3}). The proportion of Ba in the BWPs was assumed to be relatively stable, and the vehicle emissions in the tunnel were uniform. By combining the above results with filter data from sites #1 and #2, we estimated the average fleet brake wear emission factor to be 0.28 mg km^{-1} veh^{-1} (equations (9)−(11)), which is consistent with results obtained using CMB in our previous study (Table 1) [30].

The chemical compositions of filter-based PM$_{2.5}$ at sites #1 and #2 were used to evaluate the quantitative SPAMS results for ambient BWPs. A summary of the mean effective concentrations of PM$_{2.5}$ and elements at the two sites, as well as the associated mean increments and enhancement factors, are presented in Fig. S8 and Table S3. The concentrations of elements related to brake wear emissions (i.e., Ba, Cu, Fe, and Zn) are higher at site #2 than at site #1 with similar enhancement factors (Table S3), indicating that they may share similar source profiles in the tunnel. The proportions of Ba in PM$_{2.5}$ at sites #1 and #2 are 0.048% and 0.065%, respectively. According to a recent study from our group, which analyzed the chemical composition of PM$_{2.5}$ in BWPs emitted by six types of brake pads with high market shares in China, the proportion of Ba in BWP PM$_{2.5}$ was determined to be 4.9% (48.84 mg g^{-1}) [27]. Using this Ba to PM ratio, the concentrations of BWPs at sites #1 and #2 were calculated as 0.37 and 0.65 μg m^{-3}, accounting for 1.0% and 1.3% of PM$_{2.5}$, respectively. These values are comparable to the results obtained using SPAMS at site #3.

The BWP emission factor of the average fleet determined in this work is lower than that of previous dynamometer tests and the emission inventory results from the European Environment Agency (EEA), United States Environmental Protection Agency (USEPA), and National Atmospheric Emissions Inventory (NAEI) (Table 1). A reason for this discrepancy could be the relatively low frequency of braking in the tunnel compared with that in typical urban traffic conditions [4]. Nevertheless, our work quantified real-world BWP emissions by adopting a new perspective, namely, using SPAMS, thus providing an important reference for accurate assessments of brake wear emissions.

4. Conclusions

The single-particle mass spectral features and real-world emissions of BWPs were obtained using SPAMS. The main conclusions of this study are as follows:

(1) Pure BWPs mainly included Ba-containing particles, mineral particles, and carbon-containing particles, accounting for 44.2%, 43.4%, and 10.3% of the total BWPs number concentration, respectively. Larger particles mostly comprised Ba-containing particles and mineral particles, which were mainly produced by mechanical processes. In contrast, the proportion of carbon-containing particles was higher in the size range of ≤ 0.5 μm, indicating that these particles may be generated from the volatilization and condensation of organic vapors.

(2) The Ba-containing particles in the tunnel were identified based on the indicator ion at $m/z = 138$ (Ba$^+$). Ba-containing particles detected inside the tunnel and in the laboratory had similar mass spectral features and size distributions, indicating that Ba-containing particles could serve as a quantitative indicator of BWPs in ambient air. According to the experimental results and tunnel measurements, a new method for quantifying real-world BWP emissions using SPAMS was established.
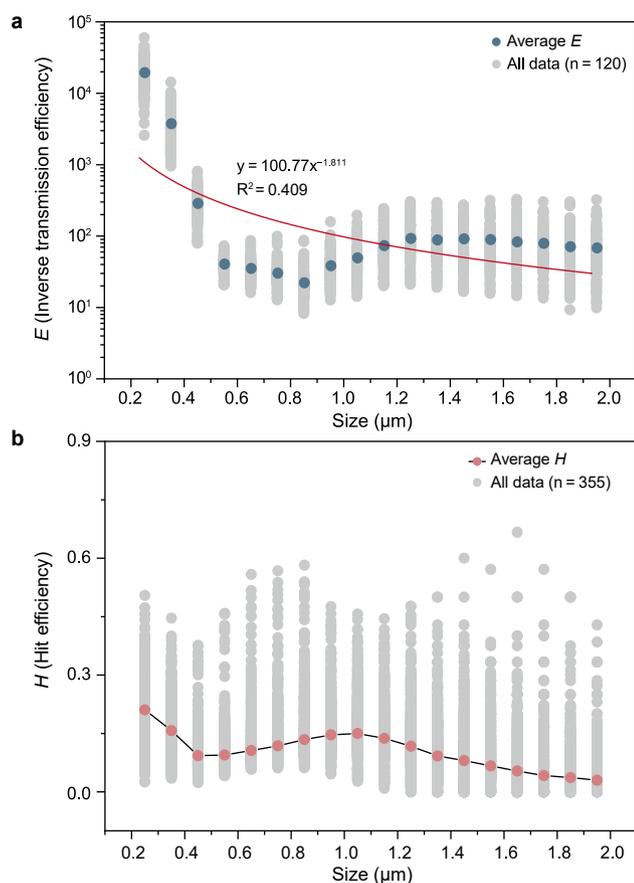
Fig. 7. a, Inverse transmission efficiency determined by SMPS and APS (size = 0.2−2.0 μm, average E_b in each size bin b, $n = 120$). **b**, Hit efficiency, defined as the ratio between the particles with mass spectral information ($N_{b,mass}$) and the particles with size information ($N_{b,SIZE}$) (hourly H_b in each size bin b, $n = 355$).

Table 1
Comparisons of brake wear PM$_{2.5}$ emission factors (mg km^{-1} veh^{-1}).

Measurement/Data source	Method	Emission factor	Reference
Tunnel	Measured directly	0.28	This study
Tunnel	CMB	0.2 ± 0.1	[30]
Roadside	CMB	0−5	[67]
Brake dynamometer	Measured directly	1.8−2.8	[68]
Brake dynamometer	Measured directly	3.9	[69]
Brake dynamometer	Measured directly	0.04−1.2	[19]
Brake dynamometer	Measured directly	0.2−1.2	[70]
Emission inventory	COPERT	2.9	[71]
Emission inventory	MOVES	2.3	[72]
Emission inventory	COPERT	3	[73]

(3) The average BWP concentration in the tunnel was 1.9 μg m^{-3}, which corresponded to approximately 4.0% of the PM$_{2.5}$ in the tunnel. Combining SPAMS measurements with filter data allowed us to estimate that the average fleet brake wear emission factor was 0.28 mg km^{-1} veh^{-1}, which was consistent with the results obtained using the CMB model.

Despite these positive conclusions, this study also had certain limitations. For example, different types of brake pads may generate different proportions of Ba-containing particles, which could introduce uncertainty into the scaling approach. Additionally, there are few direct measurements of BWP density, which might lead to uncertainty in our diameter conversion and mass calculations. Future investigations into these aspects would further improve the reliability of the evaluation results. Nevertheless, this study presents a new perspective for investigating the single-particle properties of BWPs and estimating their contributions to ambient PM based on single-particle information. The proposed method could significantly reduce the uncertainty associated with estimating BWP contributions, particularly in complex atmospheric environments. More importantly, information related to the single-particle mass spectra provides an important reference for assessing the health risks of BWPs and the potential heterogeneous chemical processes involving BWPs, both of which are highly influenced by the single-particle chemical composition [74]. This information is crucial considering the rising contribution of BWPs in urban atmospheres worldwide [9]. Future applications of this approach are not limited to tunnel observations; it can also be extended to BWP measurements under diverse atmospheric conditions, such as roadside, street canyon, and urban background environments. Additional research results using this approach will guide central and local governments in developing BWP control measures.

CRediT authorship contribution statement

Jiayuan Liu: Methodology, Investigation, Writing-Original Draft. **Jianfei Peng:** Conceptualization, Writing-Review & Editing. **Zhengyu Men:** Methodology, Investigation, Formal analysis. **Tiange Fang:** Investigation, Resources. **Jinsheng Zhang:** Methodology, Investigation, Formal analysis. **Zhuofei Du:** Data curation, Formal analysis. **Qijun Zhang:** Investigation. **Ting Wang:** Data curation. **Lin Wu:** Data curation, Supervision. **Hongjun Mao:** Funding acquisition, Project administration, Conceptualization.

Declaration of competing interest

The authors declare that they have no known competing financial interests or personal relationships that could have appeared to influence the work reported in this paper.

Appendix A. Supplementary data

Supplementary data to this article can be found online at https://doi.org/10.1016/j.ese.2023.100240.

References

[1] J.F. Peng, M. Hu, Z.F. Du, Y.H. Wang, J. Zheng, W.B. Zhang, Y.D. Yang, Y.H. Qin, R. Zheng, Y. Xiao, Y.S. Wu, S.H. Lu, Z.J. Wu, S. Guo, H.J. Mao, S.J. Shuai, Gasoline aromatics: a critical determinant of urban secondary organic aerosol formation, Atmos. Chem. Phys. 17 (17) (2017) 10743−10752.
[2] H.Y. Man, H. Liu, H. Niu, K. Wang, F.Y. Deng, X.T. Wang, Q. Xiao, J.M. Hao, VOCs evaporative emissions from vehicles in China: species characteristics of different emission processes, Environ. Sci. Ecotechnol. 1 (2020), 100002.
[3] V. Singh, A. Biswal, A.P. Kesarkar, S. Mor, K. Ravindra, High resolution vehicular PM$_{10}$ emissions over megacity Delhi: relative contributions of exhaust and non-exhaust sources, Sci. Total Environ. 699 (2020), 134273.
[4] P. Pant, R.M. Harrison, Estimation of the contribution of road traffic emissions to particulate matter concentrations from field measurements: a review, Atmos. Environ. 77 (2013) 78−97.
[5] T. Grigoratos, G. Martini, Brake wear particle emissions: a review, Environ. Sci. Pollut. Res. 22 (2015) 2491−2504.
[6] S. Wahid, Automotive brake wear: a review, Environ. Sci. Pollut. Res. 25 (2018) 174−180.
[7] S. Lawrence, R. Sokhi, K. Ravindra, Quantification of vehicle fleet PM$_{10}$ particulate matter emission factors from exhaust and non-exhaust sources using tunnel measurement techniques, Environ. Pollut. 210 (2016) 419−428.
[8] A. Piscitello, C. Bianco, A. Casasso, R. Sethi, Non-exhaust traffic emissions: sources, characterization, and mitigation measures, Sci. Total Environ. 766 (2021), 144440.
[9] F. Amato, F.R. Cassee, H.A.C.D. van der Gon, R. Gehrig, M. Gustafsson, W. Hafner, R.M. Harrison, M. Jozwicka, F.J. Kelly, T. Moreno, A.S.H. Prevot, M. Schaap, J. Sunyer, X. Querol, Urban air quality: the challenge of traffic non-exhaust emissions, J. Hazard Mater. 275 (2014) 31−36.
[10] Y. Liu, H.B. Chen, Y. Li, J.B. Gao, K. Dave, J.Y. Chen, T.Z. Li, R. Tu, Exhaust and non-exhaust emissions from conventional and electric vehicles: a comparison of monetary impact values, J. Clean. Prod. 331 (2022), 129965.
[11] Air Quality Expert Group, Non-exhaust Emissions from Road Traffic, 2019.
[12] F. Amato, O. Favez, M. Pandolfi, A. Alastuey, X. Querol, S. Moukhtar, B. Bruge, S. Verlhac, J.A.G. Orza, N. Bonnaire, T. Le Priol, J.F. Petit, J. Sciare, Traffic induced particle resuspension in Paris: emission factors and source contributions, Atmos, Environ 129 (2016) 114−124.
[13] H. Jeong, J.S. Ryu, K. Ra, Characteristics of potentially toxic elements and multi-isotope signatures (Cu, Zn, Pb) in non-exhaust traffic emission sources, Environ. Pollut. 292 (2022) (Part A).
[14] R.M. Harrison, A.M. Jones, J. Gietl, J.X. Yin, D.C. Green, Estimation of the contributions of brake dust, tire wear, and resuspension to nonexhaust traffic particles derived from atmospheric measurements, Environ. Sci. Technol. 46 (2012) 6523−6529.
[15] G. Perricone, M. Alemani, I. Metinöz, V. Matejka, J. Wahlström, U. Olofsson, Towards the ranking of airborne particle emissions from car brakes-A system

approach, Proc. Inst. Mech. Eng. - Part D J. Automob. Eng. 231 (2017) 781−797.

[16] S. Hasheminassab, M.H. Sowlat, P. Pakbin, A. Katzenstein, J. Low, A. Polidori, High time-resolution and time-integrated measurements of particulate metals and elements in an environmental justice community within the Los Angeles Basin: spatio-temporal trends and source apportionment, Atmos. Environ.-X 7 (2020), 100089.

[17] EEA, Air Quality in Europe-2019 Report, EEA Report No 10/2019, European Environment Agency, Denmark, 2019a.

[18] C.H. Jeong, J.M. Wang, N. Hilker, J. Debosz, U. Sofowote, Y.S. Su, M. Noble, R.M. Healy, T. Munoz, E. Dabek-Zlotorzynska, V. Celo, L. White, C. Audette, D. Herod, G.J. Evans, Temporal and spatial variability of traffic-related PM$_{2.5}$ sources: comparison of exhaust and non-exhaust emissions, Atmos. Environ. 198 (2019) 55−69.

[19] H. Hagino, M. Oyama, S. Sasaki, Laboratory testing of airborne brake wear particle emissions using a dynamometer system under urban city driving cycles, Atmos. Environ. 131 (2016) 269−278.

[20] S. Vasiljevic, J. Glisovic, B. Stojanovic, N. Stojanovic, I. Grujic, The analysis of the influential parameters that cause particles formation during the braking process: a review, P I Mech. Eng. J-J. Eng. 236 (2022) 31−48.

[21] C. Menapace, A. Mancini, M. Federici, G. Straffelini, S. Gialanella, Character-ization of airborne wear debris produced by brake pads pressed against HVOF-coated discs, Friction 8 (2020) 421−432.

[22] N. Stojanovic, J. Glisovic, O.I. Abdullah, A. Belhocine, I. Grujic, Particle forma-tion due to brake wear, influence on the people health and measures for their reduction: a review, Environ. Sci. Pollut. Res. 29 (2022) 9606−9625.

[23] Y.K. Ma, S. Mummullage, B. Wijesiri, P. Egodawatta, J. McGree, G.A. Ayoko, A. Goonetilleke, Source quantification and risk assessment as a foundation for risk management of metals in urban road deposited solids, J. Hazard Mater. 408 (2021), 124912.

[24] T. Gonet, B.A. Maher, I. Nyiro-Kosa, M. Posfai, M. Vaculik, J. Kukutschova, Size-resolved, quantitative evaluation of the magnetic mineralogy of airborne brake-wear particulate emissions, Environ. Pollut. 288 (2021), 117808.

[25] F.H.F.Z. Hagen, M. Mathissen, T. Grabiec, T. Hennicke, M. Rettig, J. Grochowicz, R. Vogt, T. Benter, Study of brake wear particle emissions: impact of braking and cruising conditions, Environ. Sci. Technol. 53 (2019) 5143−5150.

[26] M. Rahimi, D. Bortoluzzi, J. Wahlstrom, Input parameters for airborne brake wear emission simulations: a comprehensive review, Atmosphere 12 (2021) 7.

[27] Z.Y. Men, X.F. Zhang, J.F. Peng, J. Zhang, T.G. Fang, Q.Y. Guo, N. Wei, Q.J. Zhang, T. Wang, L. Wu, H.J. Mao, Determining factors and parameterization of brake wear particle emission, J. Hazard Mater. 434 (2022), 128856.

[28] F.H.F. zum Hagen, M. Mathissen, T. Grabiec, T. Hennicke, M. Rettig, J. Grochowicz, R. Vogt, T. Benter, On-road vehicle measurements of brake wear particle emissions, Atmos. Environ. 217 (2019), 116943.

[29] N. Bukowiecki, P. Lienemann, M. Hill, M. Furger, A. Richard, F. Amato, A.S.H. Prevot, U. Baltensperger, B. Buchmann, R. Gehrig, PM$_{10}$ emission factors for non-exhaust particles generated by road traffic in an urban street canyon and along a freeway in Switzerland, Atmos, Environ 44 (2010) 2330−2340.

[30] J.S. Zhang, J.F. Peng, C.B. Song, C. Ma, Z.Y. Men, J.H. Wu, L. Wu, T. Wang, X.F. Zhang, S.C. Tao, S.H. Gao, P.K. Hopke, H.J. Mao, Vehicular non-exhaust particulate emissions in Chinese megacities: source profiles, real-world emission factors, and inventories, Environ. Pollut. 266 (2020), 115268.

[31] M. Mathissen, T. Grigoratos, T. Lande, R. Vogt, Brake wear particle emissions of a passenger car measured on a chassis dynamometer, Atmosphere 10 (2019) 9.

[32] J. Wahlström, U. Olofsson, A field study of airborne particle emissions from automotive disc brakes, Proc. Inst. Mech. Eng. - Part D J. Automob. Eng. 229 (2014) 747−757.

[33] L.R. Crilley, F. Lucarelli, W.J. Bloss, R.M. Harrison, D.C. Beddows, G. Calzolai, S. Nava, G. Valli, V. Bernardoni, R. Vecchi, Source apportionment of fine and coarse particles at a roadside and urban background site in London during the 2012 summer ClearfLo campaign, Environ. Pollut. 220 (2017) 766−778.

[34] C. Hou, L. Shao, W. Hu, D. Zhang, C. Zhao, J. Xing, X. Huang, M. Hu, Charac-teristics and aging of traffic-derived particles in a highway tunnel at a coastal city in southern China, Sci. Total Environ. 619 (2018) 1385−1393.

[35] C.H. Xie, Y. He, L. Lei, W. Zhou, J.J. Liu, Q.Q. Wang, W.Q. Xu, Y.M. Qiu, J. Zhao, J.X. Sun, L. Li, M. Li, Z. Zhou, P.Q. Fu, Z.F. Wang, Y.L. Sun, Contrasting mixing state of black carbon-containing particles in summer and winter in Beijing, Environ. Pollut. 263 (2020), 114455.

[36] Y. Zhang, C.L. Pei, J.W. Zhang, C.L. Cheng, X.F. Lian, M.B. Chen, B. Huang, Z. Fu, Z. Zhou, M. Li, Detection of polycyclic aromatic hydrocarbons using a high performance-single particle aerosol mass spectrometer, J. Environ. Sci. 124 (2023) 806−822.

[37] J. Xu, M. Li, G.L. Shi, H.T. Wang, X. Ma, J.H. Wu, X.R. Shi, Y.C. Feng, Mass spectra features of biomass burning boiler and coal burning boiler emitted particles by single particle aerosol mass spectrometer, Sci. Total Environ. 598 (2017) 341−352.

[38] Y. Chen, H.W. Liu, R.J. Huang, F.M. Yang, M. Tian, X.J. Yao, Z.X. Shen, L.L. Yan, J.J. Cao, Atmospheric processing of loess particles in a polluted urban area of northwestern China, J. Geophys. Res. Atmos. 124 (2019) 7919−7929.

[39] J. Yang, S.X. Ma, B. Gao, X.Y. Li, Y.J. Zhang, J. Cai, M. Li, L.A. Yao, B. Huang, M. Zheng, Single particle mass spectral signatures from vehicle exhaust par-ticles and the source apportionment of online PM$_{2.5}$ by single particle aerosol mass spectrometry, Sci. Total Environ. 593 (2017) 310−318.

[40] Q. Xiao, M. Li, H. Liu, M.L. Fu, F.Y. Deng, Z.F. Lv, H.Y. Man, X.X. Jin, S. Liu, K.B. He, Characteristics of marine shipping emissions at berth: profiles for particulate matter and volatile organic compounds, Atmos. Chem. Phys. 18 (2018) 9527−9545.

[41] H.Y. Fu, M. Zheng, C.Q. Yan, X.Y. Li, H.W. Gao, X.H. Yao, Z.G. Guo, Y.H. Zhang, Sources and characteristics of fine particles over the Yellow Sea and Bohai Sea using online single particle aerosol mass spectrometer, J. Environ. Sci. 29 (2015) 62−70.

[42] X. Peng, X.X. Liu, X.R. Shi, G.L. Shi, M. Li, J.Y. Liu, Y.Q. Huangfu, H. Xu, R.Y. Ma, W. Wang, Y.C. Feng, Source apportionment using receptor model based on aerosol mass spectra and 1 h resolution chemical dataset in Tianjin, China, Atmos, Environ 198 (2019) 387−397.

[43] L.G. Shields, D.T. Suess, K.A. Prather, Determination of single particle mass spectral signatures from heavy-duty diesel vehicle emissions for PM$_{2.5}$ source apportionment, Atmos, Environ 41 (18) (2007) 3841−3852.

[44] J. Xu, H.T. Wang, X.J. Li, Y. Li, J. Wen, J.S. Zhang, X.R. Shi, M. Li, W. Wang, G.L. Shi, Y.C. Feng, Refined source apportionment of coal combustion sources by using single particle mass spectrometry, Sci. Total Environ. 627 (2018) 633−646.

[45] J. Hu, C.G. Xie, X. Li, X. Qi, S.P. Zhu, H. Zhu, J.G. Dong, P. Cheng, Z. Zhou, Direct analysis of soil composition for source apportionment by laser ablation single-particle aerosol mass spectrometry, Environ. Sci. Technol. 55 (14) (2021) 9721−9729.

[46] D.C.S. Beddows, M. Dall'Osto, O.A. Olatunbosun, R.M. Harrison, Detection of brake wear aerosols by aerosol time-of-flight mass spectrometry, Atmos. Environ. 129 (2016) 167−175.

[47] China Association of Automobile Manufacturers, Annual Report on the Development of China Automotive Industry, 2021. http://www.caam.org.cn/chn/39/cate_77/con_5235412.html.

[48] L. Li, Z. Huang, J. Dong, M. Li, W. Gao, H. Nian, Z. Fu, G. Zhang, P. Cheng, Z. Zhou, Real time bipolar time-of-flight mass spectrometer for analyzing single aerosol particles, Int. J. Mass Spectrom. 303 (2011) 118−124.

[49] C.L. Cheng, Z.Z. Huang, C.K. Chan, Y.X. Chu, M. Li, T. Zhang, Y.B. Ou, D.H. Chen, P. Cheng, L. Li, W. Gao, Z.X. Huang, B. Huang, Z. Fu, Z. Zhou, Characteristics and mixing state of amine-containing particles at a rural site in the Pearl River Delta, China, Atmos. Chem. Phys. 18 (2018) 9147−9159.

[50] Y. Zhou, X.H.H. Huang, S.M. Griffith, M. Li, L. Li, Z. Zhou, C. Wu, J.W. Meng, C.K. Chan, P.K.K. Louie, J.Z. Yu, A field measurement based scaling approach for quantification of major ions, organic carbon, and elemental carbon using a single particle aerosol mass spectrometer, Atmos. Environ. 143 (2016) 300−312.

[51] X.Y. Qin, P.V. Bhave, K.A. Prather, Comparison of two methods for obtaining quantitative mass concentrations from aerosol time-of-flight mass spec-trometry measurements, Anal. Chem. 78 (2006) 6169−6178.

[52] M. Dall'Osto, R.M. Harrison, D.C.S. Beddows, E.J. Freney, M.R. Heal, R.J. Donovan, Single-particle detection efficiencies of aerosol time-of-flight mass spectrometry during the North Atlantic marine boundary layer experi-ment, Environ. Sci. Technol. 40 (2006) 5029−5035.

[53] C.H. Jeong, M.L. McGuire, K.J. Godri, J.G. Slowik, P.J.G. Rehbein, G.J. Evans, Quantification of aerosol chemical composition using continuous single par-ticle measurements, Atmos. Chem. Phys. 11 (2011) 7027−7044.

[54] M. Kazemimanesh, M.M. Rahman, D. Duca, T.J. Johnson, A. Addad, G. Giannopoulos, C. Focsa, A.M. Boies, A comparative study on effective den-sity, shape factor, and volatile mixing of non-spherical particles using tandem aerodynamic diameter, mobility diameter, and mass measurements, J. Aerosol Sci. 161 (2022), 105930.

[55] P.F. DeCarlo, J.G. Slowik, D.R. Worsnop, P. Davidovits, J.L. Jimenez, Particle morphology and density characterization by combined mobility and aero-dynamic diameter measurements. Part 1: Theory, Aerosol Sci. Technol. 38 (2004) 1185−1205.

[56] J. Gao, Y. Zhou, J. Wang, T. Wang, W.X. Wang, Inter-comparison of WPS^{TM}-TEOM^{TM}-MOUDI^{TM} and investigation on particle density, Environ. Sci. 9 (2007) 1929−1934 (in Chinese).

[57] M. Hu, J.F. Peng, K. Sun, D.L. Yue, S. Guo, A. Wiedensohler, Z.J. Wu, Estimation of size-resolved ambient particle density based on the measurement of aerosol number, mass, and chemical size distributions in the winter in Beijing, Environ. Sci. Technol. 46 (2012) 9941−9947.

[58] R.C. Moffet, X.Y. Qin, T. Rebotier, H. Furutani, K.A. Prather, Chemically segre-gated optical and microphysical properties of ambient aerosols measured in a single-particle mass spectrometer, J. Geophys. Res-atmos. 113 (2008), D12213.

[59] K.D. Froyd, D.M. Murphy, C.A. Brock, P. Campuzano-Jost, J.E. Dibb, J.L. Jimenez, A. Kupc, A.M. Middlebrook, G.P. Schill, K.L. Thornhill, C.J. Williamson, J.C. Wilson, L.D. Ziemba, A new method to quantify mineral dust and other aerosol species from aircraft platforms using single-particle mass spectrom-etry, Atmos. Meas. Tech. 12 (2019) 6209−6239.

[60] M.E. Levy, R.Y. Zhang, A.F. Khalizov, J. Zheng, D.R. Collins, C.R. Glen, Y. Wang, X.Y. Yu, W. Luke, J.T. Jayne, E. Olaguer, Measurements of submicron aerosols in Houston, Texas during the 2009 SHARP field campaign, J. Geophys. Res. Atmos. 118 (2013) 10518−10534.

[61] R.M. Harrison, J. Stedman, D. Derwent, New directions: why are PM$_{10}$ con-centrations in Europe not falling? Atmos. Environ. 42 (2008) 603−606.

[62] J. Prakash, G. Habib, A technology-based mass emission factors of gases and aerosol precursor and spatial distribution of emissions from on-road transport sector in India, Atmos, Environ 180 (2018) 192−205.

[63] G. Dongarra, E. Manno, D. Varrica, Possible markers of traffic-related

emissions, Environ. Monit. Assess. 154 (2009) 117–125.

[64] O. Nosko, U. Olofsson, Quantification of ultrafine airborne particulate matter generated by the wear of car brake materials, Wear 374 (2017) 92–96.

[65] F. Oroumiyeh, M. Jerrett, I. Del Rosario, J. Lipsitt, J. Liu, S.E. Paulson, B. Ritz, J.J. Schauer, M.M. Shafer, J.Q. Shen, S. Weichenthal, S. Banerjee, Y.F. Zhu, Elemental composition of fine and coarse particles across the greater Los Angeles area: spatial variation and contributing sources, Environ. Pollut. 292 (2022), 118356.

[66] L. Morawska, G. Johnson, Z.D. Ristovski, V. Agranovski, Relation between particle mass and number for submicrometer airborne particles, Atmos. Environ. 33 (13) (1999) 1983–1990.

[67] M. Abu-Allaban, J.A. Gillies, A.W. Gertler, R. Clayton, D. Proffitt, Tailpipe, resuspended road dust, and brake-wear emission factors from on-road vehicles, Atmos. Environ. 37 (2003) 5283–5293.

[68] B.D. Garg, S.H. Cadle, P.A. Mulawa, P.J. Groblicki, C. Laroo, G.A. Parr, Brake wear particulate matter emissions, Environ. Sci. Technol. 34 (2000) 4463–4469.

[69] A. Iijima, K. Sato, K. Yano, M. Kato, K. Kozawa, N. Furuta, Emission factor for antimony in brake abrasion dust as one of the major atmospheric antimony sources, Environ. Sci. Technol. 42 (2008) 2937–2942.

[70] S.H. Woo, Y. Kim, S. Lee, Y. Choi, S. Lee, Characteristics of brake wear particle (BWP) emissions under various test driving cycles, Wear 480 (2021), 203936.

[71] EEA, Airbase, The European Air Quality Database, European Environment Agency, 2019.

[72] USEPA, Brake and Tire Wear Emissions from On-Road Vehicles in MOVES2014, United States Environmental Protection Agency (USEPA), 2014. Washington DC, USA add electronic publication, https://bit.ly/3nV1WK4.

[73] NAEI, Road Transport Emission Factor from NAEI 2018, 2018. https://naei.beis.gov.uk/data/ef-transport.

[74] W.J. Li, L.Y. Shao, D.Z. Zhang, C.U. Ro, M. Hu, X.H. Bi, H. Geng, A. Matsuki, H.Y. Niu, J.M. Chen, A review of single aerosol particle studies in the atmosphere of East Asia: morphology, mixing state, source, and heterogeneous reactions, J. Clean. Prod. 112 (2016) 1330–1349.